INTERNATIONAL JOURNAL OF
NUMERICAL ANALYSIS AND MODELING
Volume 2, Number 3, Pages 283–300

CONTROL OF GEOMETRY INDUCED ERROR IN hp FINITE ELEMENT(FE) SIMULATIONS I. EVALUATION OF FE ERROR FOR CURVILINEAR GEOMETRIES

DONG XUE AND LESZEK DEMKOWICZ

(Communicated by Z. Chen)

Abstract. The paper discusses a general framework for handling curvilinear geometries in high accuracy Finite Element (FE) simulations, for both elliptic and Maxwell problems. Based on the differential manifold concept, the domain is represented as a union of geometrical blocks prescribed with globally compatible, explicit or implicit parameterizations. The idea of parametric H^1-, $H(curl)-$ and $H(div)$ - conforming elements is reviewed, and the concepts of exact geometry elements and isoparametric elements are discussed. The paper focuses then on isoparametric elements, and two ways of computing FE discretization errors: a popular one, neglecting the geometry approximation, and a precise one, utilizing the exact geometry representation. Presented numerical examples indicate the necessity of accounting for the geometry error in FE error calculations., especially for the $H(curl)$ problems.

Key Words. Geometry approximation, curvilinear hp Finite Element (FE) meshes, error evaluation, Exact Geometry Integration (EGI).

1. Introduction

The hp-adaptive FE methods are some of the most powerful methodologies for simulating complex engineering problems. These numerical methods provide optimal sequences of hp-grids that achieve exponential convergence, whereas h or p method converges only, at best algebraically [1, 6]. The advantages of hp methods are achieved by the proper choice of meshing and mapping procedures to create a finite element mesh over an arbitrary domain.

Sizable errors are introduced into the prediction of parameters when the geometric approximation is too low w.r.t. [1] the polynomial order of the discretization. [15, 16] show the importance of using properly mesh entities in high order discretization to solve partial differential equations. Current development efforts in hp methods are aimed not only at a curvilinear mesh geometry representation over curved domains [12], but also at the effective definition of meshes consisting of mixed order elements.

Solving Boundary Value Problems(BVP) in complex geometries using hp finite elements consists of a double discretization. First, a mesh is introduced in order to

Received by the editors October 13, 2003 and, in revised form, March 22, 2004.
2000 *Mathematics Subject Classification.* 35R35, 49J40, 60G40.
[1] with respect to

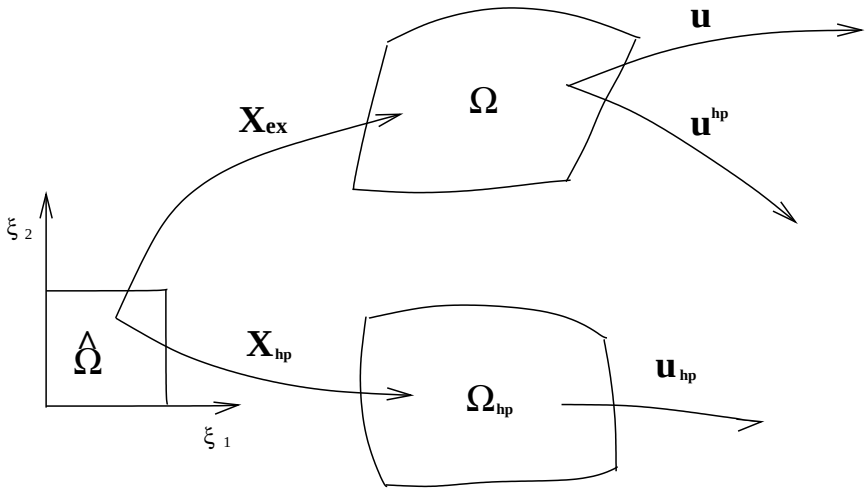

FIGURE 1. The exact and approximate domain of Finite Element Method.

create a discrete geometrical domain. Then, the solution function space is approximated by a finite dimensional function space. Both geometrical and function space approximations introduce discretization errors into the solution. The element level integral is represented abstractly as,

$$I = \int_{\Omega} \boldsymbol{K}(\boldsymbol{x}) d\boldsymbol{x} = \int_{\hat{\Omega}} \boldsymbol{K}(\boldsymbol{X}_{ex}(\boldsymbol{\xi})) d\boldsymbol{\xi}, \tag{1}$$

where K represents integrands associated with the interior of element domain Ω. The approximations can be introduced at one or more following basic functional levels: approximation of Ω, approximation of K, approximation of integration method over domain Ω. To evaluate the integral, the traditional method uses isoparametric geometry representation $\boldsymbol{X}_{hp}(\xi) \in \Omega_{hp}$, followed by the error integration on the approximate geometry domain Ω_{hp}. We will refer to it as the *Approximate Geometry Integration* (AGI),

$$\begin{aligned} I \approx I_{hp} &= \int_{\Omega_{hp}} \boldsymbol{K}_{hp}(\boldsymbol{x})\, d\,\boldsymbol{x} = \int_{\hat{\Omega}} \boldsymbol{K}_{hp}(\boldsymbol{X}_{hp}(\boldsymbol{\xi}))\, d\,\boldsymbol{\xi} \\ &\approx \sum_{\xi_l} \boldsymbol{K}_{hp}(\boldsymbol{X}_{hp}\,(\boldsymbol{\xi}_l))\omega_l. \end{aligned} \tag{2}$$

Here the weights $\boldsymbol{\omega}_l$ and quadrature points $\boldsymbol{\xi}_l$ are determined by the order of integration. Approximate geometry representation leads to inexact representation of boundary and initial conditions and, therefore, inappropriate evaluation of element level integrals. The exact solution $u : \Omega \to \mathbb{R}$ cannot be compared directly to the approximate solution $u_{hp} : \Omega_{hp} \to \mathbb{R}$ because they are computed on different physical domains, see Fig.1. This prompts us to develop a element mapping scheme resulting in a modified meaning of the FE solution defined on the exact physical domain:

$$u^{hp} : \Omega \to \mathbb{R} \tag{3}$$

Our study is primarily motivated with geometry induced error control. In this paper, we consider the following two issues:

- A proper definition of the geometry error and its assessment.

- A proper evaluation of *hp* FE discretization errors for both elliptic and Maxwell problems.

Functional error evaluation requires the study of convergence and accuracy for domains where geometric error is carefully controlled. The influence of geometry induced errors in the context of Boundary Element discretization has also been studied in [13]. The effect of geometry approximation in the p-version of the FEM has been addressed recently in [14].

A broad outline of the paper follows. Section 2 describes an element mapping scheme that exactly conforms to the curved domain with arbitrary high orders. Consideration is then given in Section 3 to a set of procedures being developed for the proper definition of geometry induced error. Section 4 analyzes the approximation error with the EGI computations for both L^2 norm and $H(curl)$ norm. Section 5 presents numerical examples for specific curved domain problems with a known exact solution for both elliptic and Maxwell problems. The results clearly demonstrate the role of the geometry approximation in the accuracy of the *hp* FE method.

2. Element mapping scheme in the *hp* FE method

In the *hp* FE simulations, a meshed geometry serves two purposes. First, it represents an arbitrary domain by a finite element mesh on which piecewise polynomial functions are defined. Second, it controls the error of approximation. The error of approximation depends on the finite element mesh and the polynomial degree of elements. In our *hp* FEM, the primary role of the meshed geometry is to represent the topological and geometric description of the object being modeled by a collection of elements. The error is controlled by both the element size h and the polynomial degree of elements p. The error is reduced as p is increased or element size h is decreased.

This paper presents a finite element mapping scheme based on an EGI geometric modeling system, *Geometrical Modeling Package* (GMP) [2, 11]. This system relates mesh entities directly to specific topological entities through an initial isotropic mesh generation scheme. The method is well suited for the *hp*-adaptive environment, because it provides direct access to the shape information of the problem domain, and makes possible to update geometry approximation during mesh refinements. The geometry representation scheme for *hp* finite elements then breaks into two parts: exact geometric modeling, and high order mesh generation.

2.1. Exact geometric modeling. The Geometrical Modeling Package provides a foundation for a multi-block *hp* mesh generator.The package allows for maintaining a continuous interface with the adaptive code to update the geometry information during mesh refinements.

In our geometric modeling, a 2D object is presented as a union of curvilinear triangles or rectangles, while a 3D object is represented with an FE-like mesh of curvilinear hexahedral blocks. The geometry of the object is prescribed then by constructing parameterizations for each of the blocks.

$$\boldsymbol{X}_G : \tilde{\Omega} \ni \boldsymbol{\eta} \rightarrow \boldsymbol{x} \in \Omega \tag{4}$$

where $\boldsymbol{\eta}$ are coordinates in reference domain $\tilde{\Omega}$; $\boldsymbol{x}$ are coordinates in physical domain Ω, see Fig.2. In GMP, each of the local edges or faces has its own global orientation. Adjusting edge and face parameterizations involves transforming local edge and face coordinates into the global ones. We handle the coordinate transformations in a hierarchical manner and ensure the *compatibility of parameterizations*. For

example, parameterizations for adjacent hexahedra is compatible if we obtain the same FE mesh when we use either of the two parameterizations of their boundary, i.e., the common rectangle.

We have explored a number of novel geometrical modeling techniques and implemented them in GMP. The GMP not only supports the construction of exact parameterizations for a general class of 2D (BEM) [9] and 3D (FEM) [10] manifolds in $\mathbb{R}^3$, but also provides the derivatives of the mappings w.r.t reference coordinates for any given points in reference frame. The two particular techniques of interest are:

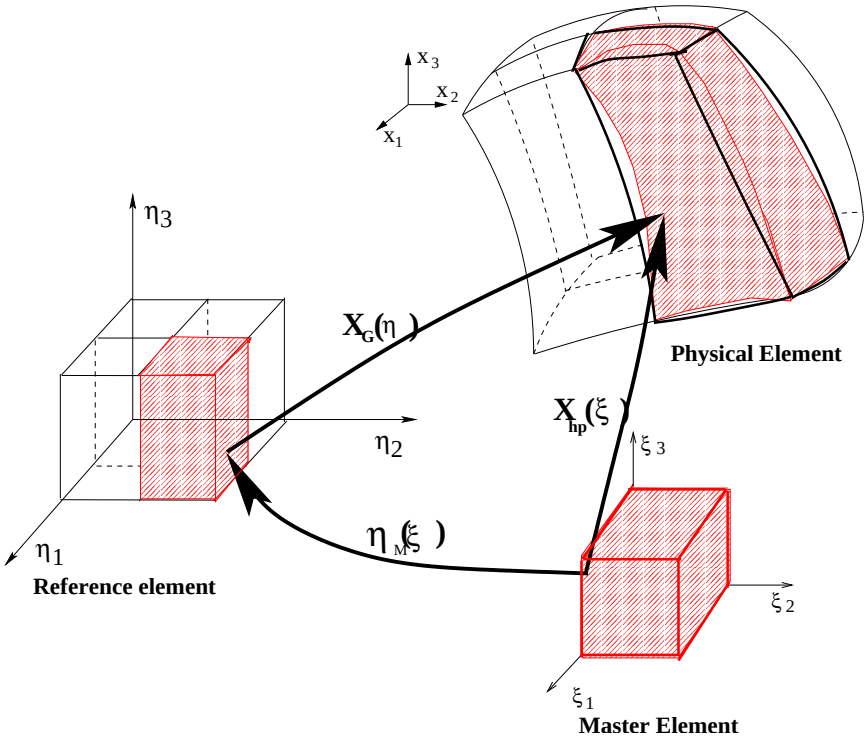

FIGURE 2. The element mapping scheme based on exact geometric representations and isotropic initial mesh generations.

- **Implicit parameterizations.**
  In this case, a map is defined implicitly by a system of nonlinear algebraic equations. In order to assess the value of the mapping for some specific choice of reference coordinates, the system has to be solved using Newton-Raphson iterations. As a result, the constructed geometric models can conform to any arbitrary high order surfaces. For example, the *implicit rectangle* lies on a given surface with its four edges cut off by four additional surfaces, see Fig. 3. Denoting the surface equations by $\varphi_i(\mathbf{x}) = 0, i =$

$1, \ldots, 5$, we introduce the following *nonlinear* equations:

$$
\begin{aligned}
\varphi_1(\mathbf{x}) &= 0 \\
(1-\eta_2)(1-f_1(\eta_1))\varphi_5(\mathbf{x}) + f_1(\eta_1)\varphi_3(\mathbf{x}) & \\
\eta_2(1-f_2(\eta_1))\varphi_5(\mathbf{x}) + f_2(\eta_1)\varphi_3(\mathbf{x}) &= 0 \\
(1-\eta_1)(1-f_3(\eta_2))\varphi_2(\mathbf{x}) + f_3(\eta_2)\varphi_4(\mathbf{x}) & \\
+\eta_1(1-f_4(\eta_2))\varphi_2(\mathbf{x}) + f_4(\eta_2)\varphi_4(\mathbf{x}) &= 0
\end{aligned} \tag{5}
$$

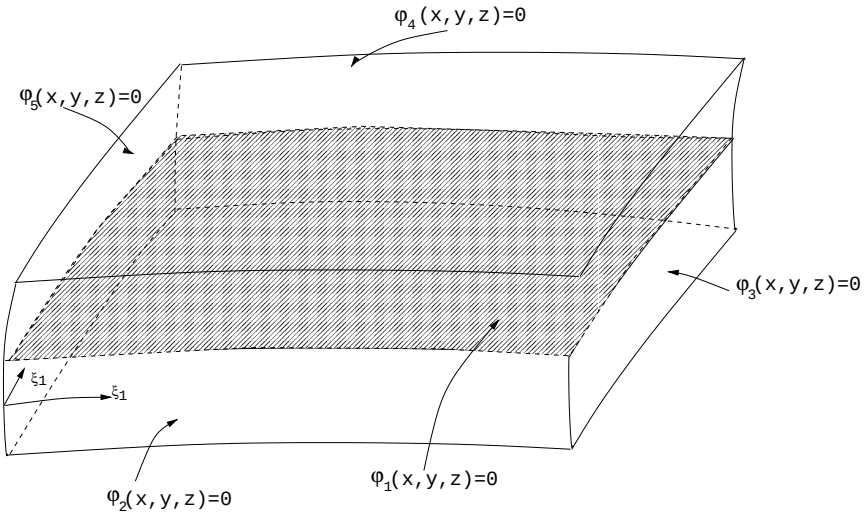

FIGURE 3. Implicit rectangle

where $f_i(\eta), i = 1, \ldots, 4$ are the *stretching functions* determined by requesting the compatibility of the rectangle parameterization with the existing, specified parameterizations for its edges:

$$
\begin{aligned}
(1-f_1(\eta_1))\varphi(\mathbf{x}_c^1(\eta_1)) + f_1(\eta_1)\varphi_3(\mathbf{x}_c^1) &= 0 \\
(1-f_2(\eta_1))\varphi(\mathbf{x}_c^3(\eta_1)) + f_2(\eta_1)\varphi_3(\mathbf{x}_c^3) &= 0 \\
(1-f_3(\eta_2))\varphi(\mathbf{x}_c^4(\eta_2)) + f_3(\eta_2)\varphi_4(\mathbf{x}_c^4) &= 0 \\
(1-f_4(\eta_2))\varphi(\mathbf{x}_c^2(\eta_2)) + f_4(\eta_2)\varphi_4(\mathbf{x}_c^2) &= 0
\end{aligned} \tag{6}
$$

with $\mathbf{x}_c^1(\eta_1), \mathbf{x}_c^2(\eta_2), \mathbf{x}_c^3(\eta_1), \mathbf{x}_c^4(\eta_2)$ being the parameterizations of the edges.

From the equation above, we can get the physical coordinates in terms of parameter η_1, η_2 The parameterization map is $\boldsymbol{X}_G(\eta_1, \eta_2)$.

- **Transfinite interpolation.**
In this case, a mapping is defined explicitly by a specific formula. The simplest examples include objects which are characterized uniquely by entities of lower dimension, and a specific interpolation rule. Thus, the geometric parameterizations can be defined by building them from the "bottom up". For instance, the parameterization of a rectangle can be obtained once we know the parameterizations for its four edges (curves). The edge parameterizations are extended to the whole reference rectangle using the classical transfinite interpolation and linear blending functions technique. Similarly, we can construct the parameterization for a transfinite interpolation hexahedron. The connectivity information includes the local ordering

of vertexes, edges and faces, and the orientations for each of the twelve edges and six faces. The hexahedron function can be written as,

$$\boldsymbol{X}_G(\boldsymbol{\eta}) = \sum_1^8 \boldsymbol{x}_v \psi_v + \sum_1^{12} \boldsymbol{\phi}_e \psi_e + \sum_1^6 \boldsymbol{\phi}_s \psi_s \tag{7}$$

where $\boldsymbol{x}_v$ denote the global physical coordinates of the vertex v; ψ_v,ψ_e and ψ_s are blending functions for vertex, edge and face respectively; $\boldsymbol{\phi}_e$ is the edge bubble function,

$$\boldsymbol{\phi}_e = \hat{\boldsymbol{\phi}}_e - \sum_{i=1}^2 \boldsymbol{x}_{v_i} \psi_{v_i}, \tag{8}$$

here $\hat{\boldsymbol{\phi}}_e$ is the GMP parametrization for the edge, adjusted for orientation; $\boldsymbol{\phi}_s$ is the face bubble function,

$$\boldsymbol{\phi}_s = \hat{\boldsymbol{\phi}}_s - \sum_{i=1}^4 \boldsymbol{x}_{v_i} \psi_{v_i} - \sum_{i=1}^4 \boldsymbol{\phi}_{e_i} \psi_{e_i}, \tag{9}$$

here $\hat{\boldsymbol{\phi}}_s$ is the GMP parameterization for the face, adjusted for orientation. (7) can be simplified as,

$$\boldsymbol{X}_G(\boldsymbol{\eta}) = \sum_1^8 \boldsymbol{x}_v \psi_v + \sum_1^{12} \hat{\boldsymbol{\phi}}_e \psi_e - \sum_1^6 \hat{\boldsymbol{\phi}}_s \psi_s \tag{10}$$

2.2. High order mesh generation. For an elliptic problem, any solution $u \in \mathbb{R}$ can be approximated as a linear combination of basis functions ϕ_i defined on physical domain Ω with unknown coefficient d.o.f.[2] u_i [29,20] ,

$$u^{hp}(\boldsymbol{x}) = \sum_{j=1}^N u_i \phi_i(\boldsymbol{x}). \tag{11}$$

The integration of element matrices is always done in terms of master element coordinates $\boldsymbol{\xi}$, therefore, it is convenient to define the shape functions on master element domain as $\hat{\phi}(\boldsymbol{\xi})$. Given a bijective map $\boldsymbol{X}_K(\boldsymbol{\xi})$, we define the H^1-conforming shape functions on the physical element as compositions of the inverse $\boldsymbol{X}_K^{-1}$ and the master element polynomial shape functions $\hat{\phi}$,

$$\phi(\boldsymbol{x}) = \hat{\phi}(\boldsymbol{\xi}) = \hat{\phi}(\boldsymbol{X}_K^{-1}(\boldsymbol{x})) = (\hat{\phi} \circ \boldsymbol{X}_K^{-1})(\boldsymbol{x}) \tag{12}$$

Eq.(12) is a classical framework for the specification and evaluation of high order shape functions on FE meshes. The element mapping that transforms a master element onto a physical element, $\boldsymbol{X}_K(\boldsymbol{\xi}) : \boldsymbol{\xi} \in \hat{\Omega} \rightarrow \boldsymbol{x} \in \Omega$, is necessary for solving partial differential equations over a curved domain. Element map $\boldsymbol{X}_K(\boldsymbol{\xi})$ can either be used directly during element computations, or approximated to construct element-level geometric approximations.

In the *hp* method, the mesh generators are based on a consistent representation of the domain as a manifold, with underlying global maps parameterizing portions of the domain. Section 2.1 depicts the scheme used to construct map $\boldsymbol{X}_G$ from reference element $\tilde{\Omega}$ to physical domain Ω. The reference hexahedron in Fig.2 is divided into a $2 \times 2 \times 1$ uniform grid. Any element in the grid (the red hexahedron

[2]degrees of freedom

in Fig.2) has a corresponding affine map from a master hexahedron element to the reference hexahedron element,

$$\boldsymbol{\eta}_M : \hat{\Omega} \ni \boldsymbol{\xi} \rightarrow \boldsymbol{\eta} \in \tilde{\Omega}. \tag{13}$$

Besides the number of subdivisions, we specify the corresponding order of approximation, which may vary from one GMP entity to another.

Fig.2 depicts two geometric mapping schemes that can be used to in high order FE computations: the *isoparametric element* (the red hexahedron in physical domain) and the *exact geometry element* (the underlying black hexahedron in physical domain.)

In the isoparametric element mesh, the approximation of the exact geometry is done with the same polynomials as those used to approximate the solution in Eq.(11). The components of the transformation map $\boldsymbol{X}_K$ come from the space of the H^1-conforming master element shape functions,

$$\boldsymbol{X}_K = \boldsymbol{X}_I(\boldsymbol{\xi}) = \sum_{j=1}^{N} \boldsymbol{x}_j \hat{\phi}_j(\boldsymbol{\xi}). \tag{14}$$

Here $\boldsymbol{x}_j$ denote geometry d.o.f obtained by projection-based interpolation [21, 22], and $\boldsymbol{X}_I(\boldsymbol{\xi}) \in \Omega_{hp}$. The parametric element shape functions can reproduce any linear function $a_j x_j$. As isoparametric elements reproduce also constants, the space of the shape functions contains the space of all linear polynomials in $\boldsymbol{x}$. However, the isoparametric element mesh, in general,does not reproduce the exact shape of the curvilinear domain. In Fig.2, the red curvilinear hexahedron does not physically match the underlying black hexahedron. Thus, it may be essential to use advanced mapping procedures so that the domain geometry is more precisely represented and integrated into FE computations.

The exact geometry element mesh provides an ideal means to construct the map $\boldsymbol{X}_K(\boldsymbol{\xi}) \in \Omega$ based on the shape of the curvilinear domain boundary entities within the GMP. Upon a change of variables, the original problem can then be redefined in the reference domain discretized with affine elements. The desired map can be obtained as

$$\boldsymbol{X}_K = \boldsymbol{X}_G(\boldsymbol{\eta}(\boldsymbol{\xi})). \tag{15}$$

In this case, the exact mathematical representation of the curvilinear domain is expressed within the reference element framework with corresponding order of approximation for each subelement. The association of mesh topological entities w.r.t. the topological entities of the geometric model, is central to obtain the shape information for individual mesh entities in Eq.(12).

2.3. Parametric elements. This paper focuses on the geometrical modeling issues in context of two classes of PDEs: elliptic problems and Maxwell problems. In order to solve the Maxwell's equations using finite elements, a family of $H(\mathbf{curl})$ conforming elements is needed, since the space of admissible solutions $\boldsymbol{E}$ is contained in $H(\mathbf{curl})$. Nedelec introduced two families of finite elements that conform in $H(\mathbf{curl}, \Omega) = \{\boldsymbol{E} \in \boldsymbol{L}^2(\Omega) : \boldsymbol{\nabla} \times \boldsymbol{E} \in \boldsymbol{L}^2(\Omega)\}$, $\Omega \subset \mathbb{R}^3$ [3, 4]. The relation between the two spaces, H^1 and $\boldsymbol{H}(curl)$, is part of a more general *exact sequence* of spaces and operators,

$$\mathbb{R} \longrightarrow H^1 \xrightarrow{\boldsymbol{\nabla}} \boldsymbol{H}(\mathrm{curl}) \xrightarrow{\boldsymbol{\nabla}\times} \boldsymbol{H}(\mathrm{div}) \xrightarrow{\boldsymbol{\nabla}\circ} L^2 \longrightarrow 0. \tag{16}$$

Recall that, in an exact sequence of operators, the range of each operator coincides with the null space of the next operator in the sequence.

The exact sequence property is crucial in proving stability for the variational formulation for the time- harmonic Maxwell equations. This suggest that the (piecewise) polynomial Finite Element discretization of the $H(\text{curl})$ space should be constructed in such a way that the exact sequence property is also satisfied at the discrete level. The *de Rham* diagram [5, 7] relates then the two exact sequences of spaces, on both continuous and discrete levels, and the corresponding interpolation operators.

To keep the exact sequence property, we define the $\boldsymbol{H}(\text{curl})$-, $\boldsymbol{H}(\text{div})$-conforming elements according to transformation rule (12). The transformation rule for gradients implies the transformation rule for $\boldsymbol{H}(\text{curl})$ conforming elements,

$$\begin{aligned} \frac{\partial u}{\partial x_i}(\boldsymbol{x}) &= \sum_{k=1}^{3} \frac{\partial \hat{u}}{\partial \xi_k} \frac{\partial \xi_k}{\partial x_i} \\ E_i(\boldsymbol{x}) &= \sum_{k=1}^{3} \hat{E}_k(\boldsymbol{\xi}) \frac{\partial \xi_k}{\partial x_i}, \end{aligned} \tag{17}$$

where E_i are components of the admissible solutions $\boldsymbol{E} \in \boldsymbol{H}(\text{curl}, \Omega)$, with corresponding $\hat{E}_k$ defined on the master element $\hat{\Omega}$. The transformation rule for the curl operator implies similarly the transformation rule for the $\boldsymbol{H}(\text{div})$-conforming elements,

$$\begin{aligned} (\nabla \times E)_i(\boldsymbol{x}) &= \sum_{k=1}^{3} J^{-1} \frac{\partial x_i}{\partial \xi_k} (\nabla \times \hat{E})_k(\boldsymbol{\xi}) \\ H_i(\boldsymbol{x}) &= \sum_{k=1}^{3} J^{-1} \frac{\partial x_i}{\partial \xi_k} \hat{H}_k(\boldsymbol{\xi}), \end{aligned} \tag{18}$$

where J^{-1} is the inverse Jacobian. Defining the parametric element spaces using the transformation rules listed above, we preserve for the parametric element the exact sequence in Eq.(16). The *hp*-edge elements, resulting from the $H(\mathbf{curl})$-conforming FE approximation, involve the implementation of vector-valued shape functions with different d.o.f., in order to take into account tangential and normal components of the electric field [8, 7].

3. Geometry discretization error

The approximation error depends both on the finite element mesh and the polynomial degree of elements. The accuracy of geometry approximation is a key issue which must be accounted for, during element level computations within an adaptive environment. Since the available theory is unable to specifically quantify the influence of the geometry approximation, a simple numerical study was performed. To assess the quality of the isoparametric approximation of exact geometry, we define the geometry error function as,

$$\boldsymbol{\delta}(\boldsymbol{x}) = \mathbf{id}(\mathbf{x}) - \boldsymbol{X}^{hp}(\boldsymbol{x}) \tag{19}$$

where function $\boldsymbol{X}^{hp}$ represents the approximate geometry map defined on the physical domain. More precisely,

$$\boldsymbol{X}^{hp}(\boldsymbol{x}) = (\boldsymbol{X}_{hp} \circ \boldsymbol{\eta}_M^{-1} \circ \boldsymbol{X}_G^{-1})(\boldsymbol{x}) = \boldsymbol{X}_{hp}(\boldsymbol{\xi}), \tag{20}$$

where

$$\boldsymbol{X}_G(\boldsymbol{\eta}_M(\boldsymbol{\xi})) = \boldsymbol{x}. \tag{21}$$

In a rather arbitrary way, we choose the H^1-(semi) norm to measure the geometry error, (according to FE error analysis [23], the $W^{1,\infty}$ norm would a better choice), and report always the geometry error related to the norm of the exact geometry element map,

$$\mathcal{E}_{g,H^1} = \frac{||\boldsymbol{\delta}||_{H^1(\Omega)}}{||\mathbf{id}(\boldsymbol{x})||_{H^1(\Omega)}}, \tag{22}$$

where $||\mathbf{id}(\boldsymbol{x})||_{H^1(\Omega)}$ is equal to three times of the volume of Ω. The H^1 semi norm of the geometry error function is evaluated on the corresponding reference domain $\tilde{\Omega}$ by using GMP parametrization and the affine map $\boldsymbol{\eta}_M$,

$$\begin{aligned} ||\mathbf{id} - \boldsymbol{x}^{hp}||_{H^1} &= ||\boldsymbol{\delta}||_{H^1} = \left(\int_\Omega \left(\frac{\partial(\mathbf{id} - \boldsymbol{x}^{hp})}{\partial \boldsymbol{x}} \right)^2 d\boldsymbol{x} \right)^{1/2} \\ &= \left(\int_{\tilde{\Omega}} \left[\sum_{k=1}^{3} \sum_{l=1}^{3} a_{kl} \frac{\partial \boldsymbol{\delta}}{\partial \eta_k} \frac{\partial \boldsymbol{\delta}}{\partial \eta_l} \right] J_1 d\boldsymbol{\eta} \right)^{1/2}. \end{aligned} \tag{23}$$

The derivatives of $\boldsymbol{\delta}$ w.r.t. reference coordinates are calculated as follows,

$$\frac{\partial \boldsymbol{\delta}}{\partial \eta_i}(\boldsymbol{\eta}) = \frac{\partial \boldsymbol{X}_G}{\partial \eta_i}(\boldsymbol{\eta}) - \sum_{j=1}^{N} \boldsymbol{x}_j \sum_{k=1}^{3} \frac{\partial \hat{\phi}_j}{\partial \xi_k}(\boldsymbol{\xi}) \frac{\partial \xi_k}{\partial \eta_i}(\boldsymbol{\eta}); \tag{24}$$

where $\boldsymbol{\eta}_M(\boldsymbol{\xi}) = \boldsymbol{\eta}$; J_1 is the Jacobian,

$$J_1 = \left| \frac{\partial \boldsymbol{x}}{\partial \boldsymbol{\eta}} \right|, \tag{25}$$

and a_{kl} is the metric resulting from the change of variables from $\boldsymbol{x}$ to $\boldsymbol{\eta}$,

$$a_{kl} = \sum_{p=1}^{3} \frac{\partial \eta_k}{\partial x_p} \frac{\partial \eta_l}{\partial x_p}. \tag{26}$$

In order to sustain the exponential rate of convergence of hp-refinements, the geometry error should also converge exponentially.

4. A precise definition of FE discretization errors

In this section, we propose a precise definition of the FE error incorporating the effects of geometry approximation. We discuss then the computation of the error for both elliptic and Maxwell boundary-value problems.

4.1. H^1 norm for elliptic problems. Solution u of an elliptic problem is contained in $H^1(\Omega)$, and the relative FE error is defined as,

$$\mathcal{E}_{s,H^1} = \frac{||u(\boldsymbol{x}) - u^{hp}(\boldsymbol{x})||_{H^1(\Omega)}}{||u(\boldsymbol{x})||_{H^1(\Omega)}}. \tag{27}$$

Here u^{hp} represents the FE solution evaluated on the *exact* geometry,

$$u^{hp}(\boldsymbol{x}) = \left(\hat{u}_{hp} \circ \boldsymbol{\eta}_M^{-1} \circ \boldsymbol{X}_G^{-1} \right)(\boldsymbol{x}) = \hat{u}_{hp}(\boldsymbol{\xi}) \tag{28}$$

where $\boldsymbol{x}$ is given by (21).

For the case of second-order elliptic equations, the first order norm can be replaced with the (equivalent) first order semi-norm,

$$||e||_{L^2} = \left(\int_\Omega \sum_{i=1}^{3} \frac{\partial e}{\partial x_i} \frac{\partial e}{\partial x_i} d\boldsymbol{x} \right)^{1/2}. \tag{29}$$

The norm of the exact solution is integrated in practice in the reference domain,

$$||u||^2_{L^2} = \int_\Omega \sum_{i=1}^{3} \frac{\partial u}{\partial x_i}\frac{\partial u}{\partial x_i} d\boldsymbol{x} = \int_{\tilde{\Omega}} \sum_{i=1}^{3} \frac{\partial u}{\partial x_i}\frac{\partial u}{\partial x_i} J_1 d\boldsymbol{\eta}. \tag{30}$$

Let $e(\boldsymbol{x})$ be the difference between exact solution and hp FE solution, $e(\boldsymbol{x}) = u(\boldsymbol{x}) - u^{hp}(\boldsymbol{x})$. We transform the difference e from physical element Ω to reference element $\tilde{\Omega}$ by using the transformation rule for the H^1-conforming element in Eq.(12),

$$\begin{aligned} e(\boldsymbol{x}) &= u(\boldsymbol{x}) - u^{hp}(\boldsymbol{x}) \\ &= (\tilde{u} \circ \boldsymbol{X}_G^{-1})(\boldsymbol{x}) - \left(\hat{u}_{hp} \circ \boldsymbol{\eta}_M^{-1} \circ \boldsymbol{X}_G^{-1}\right)(\boldsymbol{x}) \\ &= \tilde{u}(\boldsymbol{\eta}) - \sum_{i=1}^{N} u_i \hat{\phi}_i(\boldsymbol{\xi}), \end{aligned} \tag{31}$$

where $\boldsymbol{x}$ is given by (21) and $\tilde{u}(\boldsymbol{\eta}) = u(\boldsymbol{X}_G(\boldsymbol{\eta}))$. Consequently, the finite element discretization error evaluated with EGI is,

$$||e||_{H^1} = \int_{\tilde{\Omega}} \left[\sum_{k=1}^{3}\sum_{l=1}^{3} a_{kl} \frac{\partial \tilde{e}}{\partial \eta_k}\frac{\partial \tilde{e}}{\partial \eta_l} \right] J_1 d\boldsymbol{\eta},$$

where

$$\frac{\partial \tilde{e}}{\partial \eta_k} = \sum_{i=1}^{3} \frac{\partial u}{\partial x_i}\frac{\partial x_i}{\partial \eta_k} - \sum_{i=1}^{3} \frac{\partial \hat{u}^{hp}}{\partial \xi_i}\frac{\partial \xi_i}{\partial \eta_k}. \tag{32}$$

Note that $\frac{\partial x_i}{\partial \eta_k}$ and $\frac{\partial \xi_i}{\partial \eta_k}$ are derived from exact geometry map $\boldsymbol{X}_G(\boldsymbol{\eta})$ in (4) and initial mesh affine map $\boldsymbol{\eta}_M^{-1}(\boldsymbol{\eta})$ in (13), respectively. $\frac{\partial \hat{u}}{\partial \xi_i}$ are the derivatives of exact solution w.r.t. master element coordinates,

$$\frac{\partial u^{hp}}{\partial \xi_k} = \sum_{j=1}^{N} u_j \frac{\partial \hat{\phi}_j}{\partial \xi_k}. \tag{33}$$

As a result, the approximate error now can be expressed on the reference element. In order to eliminate quadrature error, we evaluate the EGI error by using an adaptive tensor-product Gaussian quadrature integration.

4.2. $H(curl)$ **norm for Maxwell problems.** The relative approximation error, measured in $H(curl)$ norm can be expressed as,

$$\mathcal{E}_{s,H(curl)} = \frac{||\boldsymbol{E}(\boldsymbol{x}) - \boldsymbol{E}^{hp}(\boldsymbol{x})||_{H(curl)}}{||\boldsymbol{E}(\boldsymbol{x})||_{H(curl)}}. \tag{34}$$

Here

$$||\boldsymbol{e}||_{H(curl)} = \left(\int_\Omega |\boldsymbol{e}|^2 + |\nabla \times \boldsymbol{e}|^2 \, d\boldsymbol{x} \right)^{1/2}.$$

In view of (19), the use of curl term in the definition indicates that the geometry induced error may have more impact on the $H(curl)$ norm.

Once the exact solution is known, the corresponding norm is evaluated by integrating on the reference domain,

$$||\boldsymbol{E}||^2_{H(curl)} = \int_{\tilde{\Omega}} \left(|\boldsymbol{E}(\boldsymbol{x}(\boldsymbol{\eta}))|^2 + |\nabla \times \boldsymbol{E}(\boldsymbol{x}(\boldsymbol{\eta}))|^2 \right) J_1 d\, \boldsymbol{\eta} \tag{35}$$

The error evaluation is more complicated for the FE error function $\boldsymbol{e}(\boldsymbol{x}) = \boldsymbol{E} - \boldsymbol{E}^{hp}$, as the FE solution involves the use of Piola-Kirchhoff transformation [10].

Integration on the physical element is performed by changing variables and moving function $\boldsymbol{e}$ from the physical to the reference element. The exact geometry $\boldsymbol{X}_G(\boldsymbol{\eta})$ in (4) is used to transform the integrals to the reference parametric elements by using transformation rule for the $H(curl)$ -conforming elements,

$$e_i(\boldsymbol{x}) = \sum_{k=1}^{3} \tilde{e}_k(\boldsymbol{\eta}) \frac{\partial \eta_k}{\partial x_i}(\boldsymbol{x}). \tag{36}$$

Equivalently,

$$\tilde{e}_k(\boldsymbol{\eta}) = \sum_{i=1}^{3} e_i(\boldsymbol{x}) \frac{\partial x_i}{\partial \eta_k}(\boldsymbol{\eta}). \tag{37}$$

Similarly, using the transformation for $\boldsymbol{H}(div)$-conforming elements, we have

$$(\boldsymbol{\nabla x} \times \boldsymbol{e})_i \quad = \quad J_1^{-1} \sum_{k=1}^{3} \frac{\partial x_i}{\partial \eta_k} (\boldsymbol{\nabla \eta} \times \tilde{\boldsymbol{e}})_k, \tag{38}$$

and,

$$(\boldsymbol{\nabla \eta} \times \tilde{\boldsymbol{e}})_k \quad = \quad J_1 \sum_{i=1}^{3} \frac{\partial \eta_k}{\partial x_i} (\boldsymbol{\nabla x} \times \boldsymbol{e})_i. \tag{39}$$

where Jacobian J_1 is given by (25). The finite element discretization error of $\boldsymbol{E}$ evaluated with EGI is,

$$||\boldsymbol{e}||^2_{H(curl)} \quad = \quad \int_{\tilde{\Omega}} \sum_{k=1}^{3} \sum_{l=1}^{3} \left[a_{kl} \tilde{e}_k \tilde{e}_l + b_{kl} (\boldsymbol{\nabla \eta} \times \tilde{\boldsymbol{e}})_k \cdot (\boldsymbol{\nabla \eta} \times \tilde{\boldsymbol{e}})_l \right] J_1 d\boldsymbol{\eta}, \tag{40}$$

where coefficients a_{kl} is given by (26) and b_{kl} is also obtained from exact geometry modeling framework,

$$b_{kl} = \sum_{i=1}^{3} (J_1^{-1})^2 \frac{\partial x_i}{\partial \eta_k} \frac{\partial x_i}{\partial \eta_l}. \tag{41}$$

The exact solution $\boldsymbol{E} = (E_1, E_2, E_3)$, defined on physical domain, and the FE solution $\boldsymbol{E}_{hp} = \sum_{j=1}^{N} u_j \hat{\boldsymbol{\phi}}_j$ (u_j are d.o.f.), defined on the master element, can finally both switch to the reference element coordinates $\boldsymbol{\eta}$. Since affine map $\boldsymbol{\eta}_M$ does not induce any additional error, from Eq. (18) and (19), we have

$$\tilde{e}_k(\boldsymbol{\eta}) = \sum_{i=1}^{3} E_i \frac{\partial x_i}{\partial \eta_k} - \sum_{i=1}^{3} \sum_{j=1}^{N} u_j (\hat{\phi}_j)_i \frac{\partial \xi_i}{\partial \eta_k} \tag{42}$$

and,

$$(\nabla \times \tilde{e})_k(\boldsymbol{\eta}) \quad = \quad \sum_{i=1}^{3} J_1 \frac{\partial \eta_k}{\partial x_i} (\boldsymbol{\nabla x} \times \boldsymbol{E})_i - \sum_{i=1}^{3} \sum_{j=1}^{N} J_1 \frac{\partial \eta_k}{\partial \xi_i} u_j (\boldsymbol{\nabla \xi} \times \hat{\boldsymbol{\phi}}_j)_i. \tag{43}$$

Here $(\hat{\phi}_j)_i$ and $(\boldsymbol{\nabla \xi} \times \hat{\boldsymbol{\phi}}_j)_i$ denote the ith component of the corresponding vectors.

5. Numerical Examples

We illustrate the proposed error evaluation scheme with three numerical examples for elliptic and Maxwell problems defined on a unit spherical domain. The technique is compared with a customary error evaluation procedure in which the FE discretization error is evaluated directly on the approximate geometry, neglecting the geometry approximation error.

5.1. Elliptic problems.

5.1.1. Example 1: A Dirichlet problem for the Poisson equation. A numerical example based on the solution of Poisson's equation in three dimensions illustrates the impact of the mapping scheme on the convergence rate of finite element error. Consider the solution of boundary-value problem,

$$\begin{aligned} -\triangle u(\boldsymbol{x}) &= f(\boldsymbol{x}) \qquad |\boldsymbol{x}| < 1, \\ u(\boldsymbol{x}) &= 0 \qquad\quad |\boldsymbol{x}| = 1 \end{aligned} \tag{44}$$

where Ω is a sphere of unit radius and $f(x)$ is specified such that the exact solution is

$$u(\boldsymbol{x}) = r^2(1-r^2), \qquad r = (\sum_{i=1}^{3} x_i^2)^{1/2}. \tag{45}$$

Example meshes are included to demonstrate features of the procedure. Fig.4 shows the exact solution evaluated on the initial mesh. The real physical domain Ω (unit sphere) is represented by using a coarse curvilinear mesh consisting of seven hexahedra with uniform subdivision number $1/h = 3$. The exact energy of the solution is

$$||u||_{H^1} = 4\pi \int_0^1 \left|\frac{\partial u}{\partial r}\right|^2 r^2 dr = 4\sqrt{\frac{\pi}{5}}. \tag{46}$$

We compare the relative Laplace solution error $\mathcal{E}_{s,H1}$ evaluated on the approximate domain Ω_{hp} with the one evaluated on the exact physical domain Ω, the AGI and EGI, in Fig.5. Fig. 5 also plots the relative geometry error $\mathcal{E}_{g,H1}$ versus the order of approximation p. Since the solution is smooth, the logarithm of the error is expected to decrease linearly with the approximation order p (exponential convergence). Note that the AGI error is one order of magnitude bigger than the EGI error. The EGI error curve seems also to be displaying less variation than its AGI counterpart.

5.1.2. Example2: A Neumann problem for the Laplace equation. A more complicated example for the Laplace equation is provided by the Neumann problem,

$$\begin{aligned} -\triangle u(\boldsymbol{x}) &= 0, \qquad\quad |\boldsymbol{x}| < 1 \\ \nabla_n u(\boldsymbol{x}) &= g(\boldsymbol{x}) \qquad |\boldsymbol{x}| = 1 \end{aligned} \tag{47}$$

where $g(x)$ is the Neumann boundary condition data on the sphere. Using spherical coordinates (r, θ, ϕ) in (47), the separation of variables $u = f(r)g(\theta)h(\phi)$ leads to,

- Euler equation in r

$$\frac{\partial}{\partial r}\left(r^2 \frac{\partial f(r)}{\partial r}\right) - \lambda^2 f(r) = 0 \tag{48}$$

with solutions

$$f_n(r) = a_n r^n \quad n \geq 0 \tag{49}$$

- Legendre equation in θ

$$\frac{\theta}{g(\theta)}\frac{\partial}{\partial \theta}\left(sin\theta \frac{\partial g(\theta)}{\partial \theta}\right) + \lambda^2 sin^2\theta = const \tag{50}$$

with solution

$$g_n^m(\theta) = b_{nm} P_n^m(cos\theta), \quad 0 \leq m \leq n \tag{51}$$

where $P_n^m(cos\theta)$ are Legendre functions defined in [24].

- second-order linear ordinary differential equation in ϕ

$$\frac{\partial^2 h(\phi)}{\partial \phi^2} = -\mu^2 h(\phi) \tag{52}$$

with solutions

$$h_m(\phi) = A_m cos(m\phi) + B_m sin(m\phi),\ \forall m \geq 0. \tag{53}$$

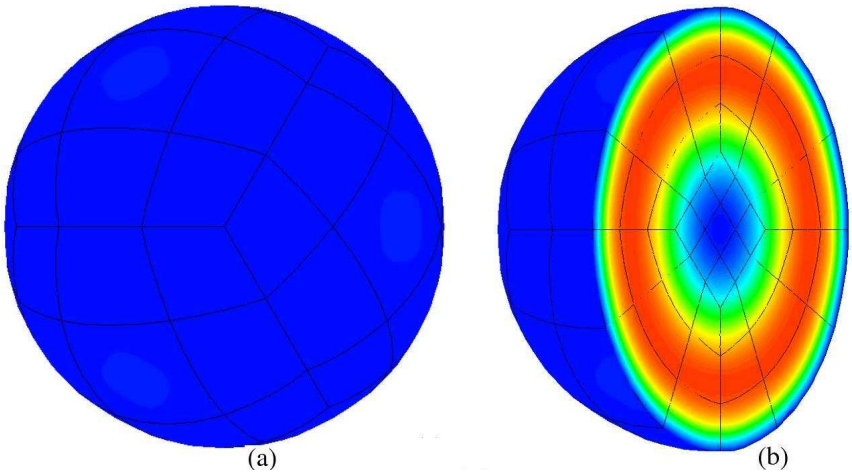

FIGURE 4. Example 1: Contour plots of the exact solution on the sphere and cross section $z = 0$

We choose,

$$g(\eta, \phi) = \sum_{m=0}^{4} P_4^m(cos\theta)(cos(m\phi) + sin(m\phi)). \tag{54}$$

The corresponding exact solution is then

$$u(r, \eta, \phi) = \sum_{m=0}^{4} \frac{1}{4} r^4 P_4^m(cos\theta)(cos(m\phi) + sin(m\phi)). \tag{55}$$

Fig.6 shows the exact solution evaluated on the initial mesh with uniform subdivision number $1/h = 3$.

Fig. 7 plots the relative geometry error $\mathcal{E}_{g,H1}$ and the relative solution error $\mathcal{E}_{s,H1}(\boldsymbol{x})$ versus order of approximation p. The logarithm of the errors in (22) and (27) are expected to decrease linearly when the sphere is approximated with seven hexadra with quadratic, cubic, quartic and higher order element maps. In this case, the two curves are practically identical and display the expected exponential convergence rates. (The AGI error is slightly less than the EGI error.)

5.2. Maxwell problems.

5.2.1. Example 3: Plane wave. Our final example deals with a Dirichlet boundary value problem for the time-harmonic Maxwell equation in a unit spherical domain,

$$\begin{aligned} \nabla \times (\frac{1}{\mu} \nabla \times \boldsymbol{E}) - (\omega^2 \epsilon - j\omega\sigma)\boldsymbol{E} &= -j\omega J^{imp}, \quad |\boldsymbol{x}| < 1 \\ \boldsymbol{n} \times \boldsymbol{E} &= \boldsymbol{n} \times \boldsymbol{E}_0, \quad |\boldsymbol{x}| = 1. \end{aligned} \tag{56}$$

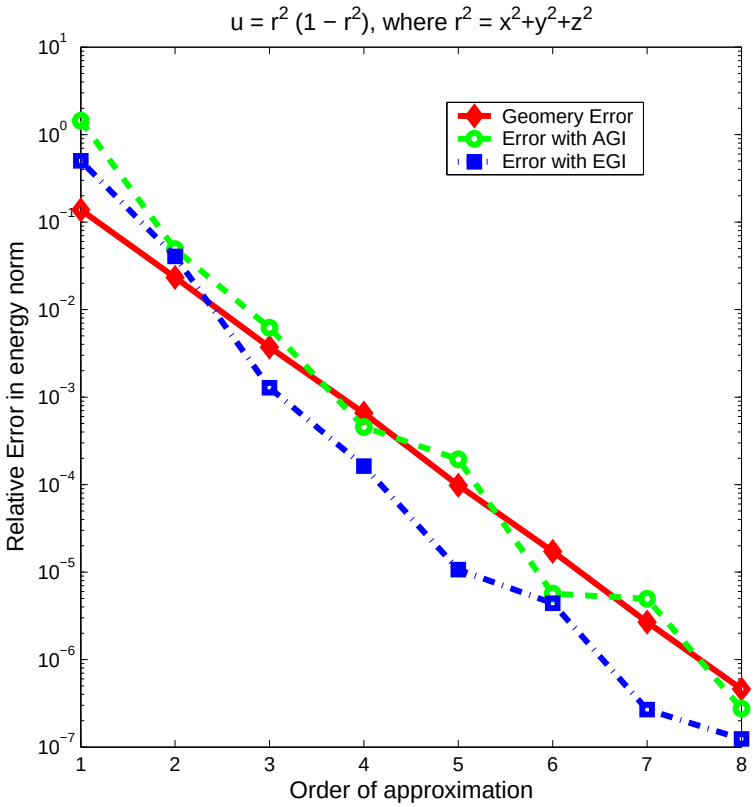

FIGURE 5. Example 1: Geometry and solution errors.

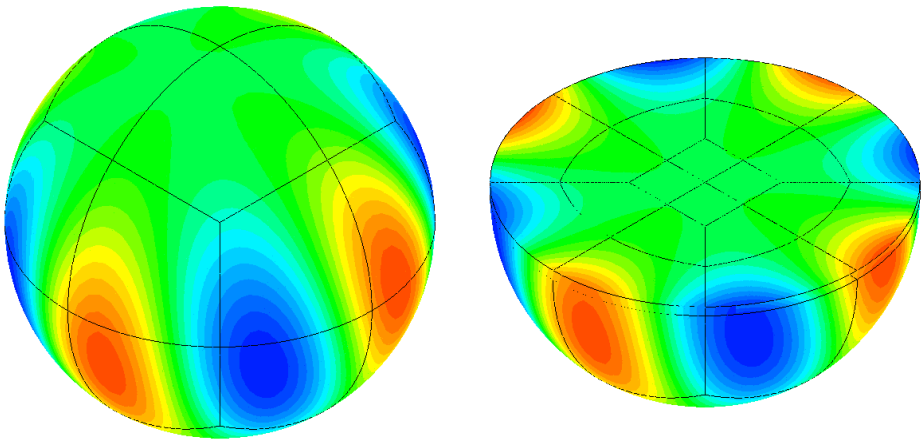

FIGURE 6. Example 2: Contour plots of the exact solution on the sphere and cross section $z = 0$

Here $\omega, \epsilon, \mu, \sigma$ denote the angular frequency, permittivity, permeability and conductivity, respectively; J^{imp} stands for an impressed surface current.

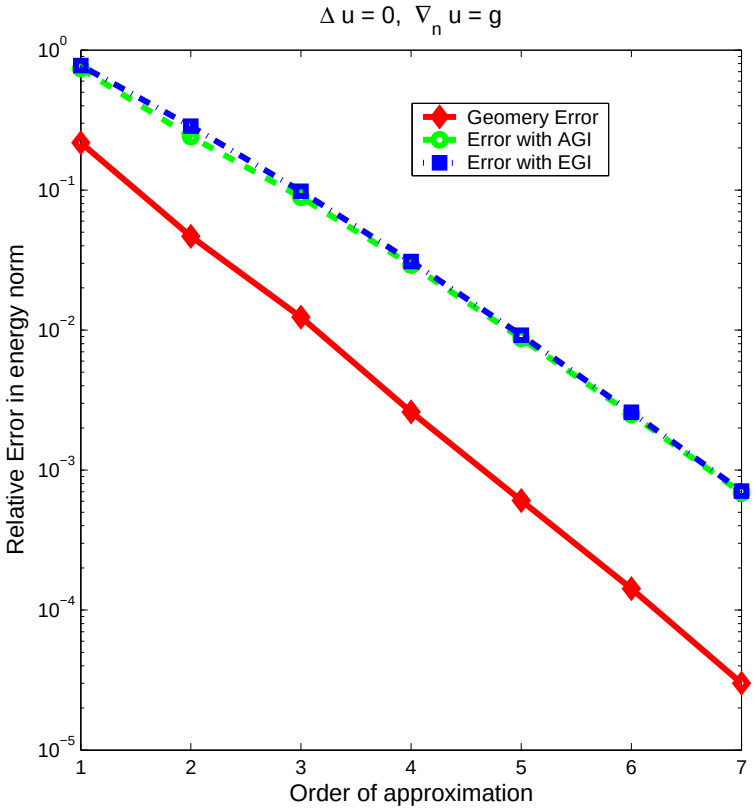

FIGURE 7. Example 2: Geometry and solution errors

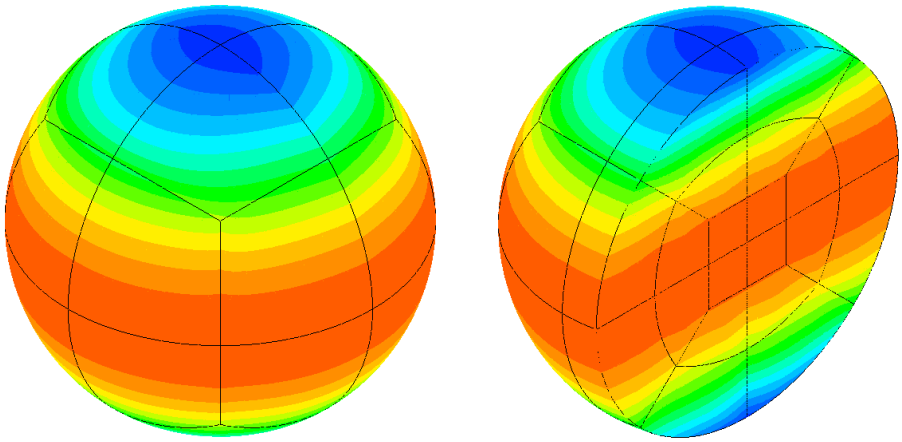

FIGURE 8. Example 3: Contour plots of the exact solution E_x on the sphere and cross section $z = 0$

A particular solution to the homogeneous ($\boldsymbol{J}^{imp} = \boldsymbol{0}$) problem with constant material data, is provided by the plane wave

$$\boldsymbol{E}(\boldsymbol{x}) = \boldsymbol{E}_0 e^{i\boldsymbol{k}\cdot\boldsymbol{x}}. \tag{57}$$

The polarization vector $\boldsymbol{E}_0 = (E_1, E_2, E_3)$ and wave vector $\boldsymbol{k} = (k_1, k_2, k_3)$ must satisfy the conditions,

$$\begin{aligned} E_1 k_1 + E_1 k_1 + E_1 k_1 &= 0 \\ k_1^2 + k_2^2 + k_3^2 &= \omega^2 \epsilon - j\omega\sigma \end{aligned} \tag{58}$$

We choose $\sigma = 0, \omega^2 \epsilon\mu = 1, \boldsymbol{k} = (0, 0, \omega\sqrt{\epsilon\mu}) = (0, 0, 1), \boldsymbol{E}_0 = (1, 0, 0)$.

Fig.8 shows the components of the exact solution evaluated on the initial mesh with uniform subdivision number $1/h = 2$. The evaluation of the error has been discussed in Section 4.2. Fig.9 shows both the geometry error and the FE errors using the two different error evaluation techniques. Both the error value and the represented convergence rates depend strongly upon the way of evaluating the error.

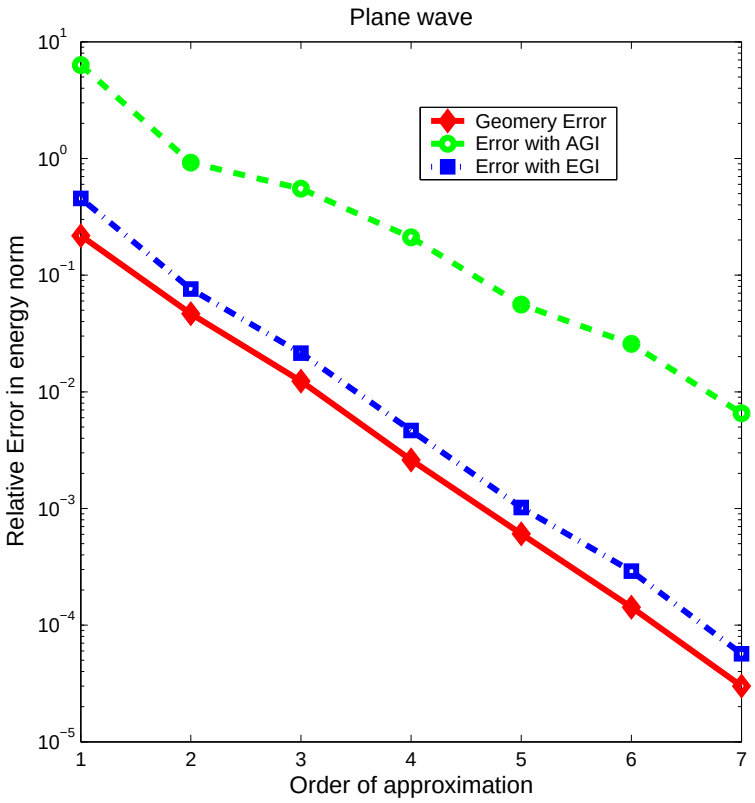

FIGURE 9. Example 3: Geometry and solution errors

6. Conclusions and future work

The paper reviews the theoretical framework for a general class of parametric H^1-, $H(curl)-$ and $H(div)$ - conforming elements, with both exact and isoparametric geometry description. A systematic way of computing the H^1- and $H(curl)-$ discretization errors, accounting for the error in geometry approximation, has been proposed. The technique has been illustrated with three numerical examples and compared with the customary error evaluation neglecting the geometry approximation error. The presented examples demonstrate that the two errors may differ

by an order in magnitude, indicating the care with which convergence results for higher order elements on curved geometries should be reported.

Future work will focus on a comparison of exact geometry and isoparametric elements and possible means to control the geometry induced errors for both CAD-based and reconstructed geometry models, focusing on a human head model with a G^1-continuous reconstructed geometry model [19, 20]. In order to simulate the absorption and diffraction of EM waves in the human head using the hp method, we intend to investigate how the G^1 regular parametrization will affect the convergence rates of high order methods. Among other tasks, the multi-resolution techniques [17, 18] and hierarchical geometry reconstruction schemes are under study to obtain a efficient and effective coarse head model conforming to fine grid representations.

Acknowledgments

The work on the human head model is being done in collaboration with Dr. Chandrajit Bajaj and Yongjie Zhang from the Computational Visualization Center (CCV) at UT Austin.

References

[1] W. Gui and I. Babuŝka, The h, p and $h-p$ Versions of the Finite Element Method in One Dimension. Part 1. The Error Analysis of the p-Version. Part 2. The Error Analysis of the h- and $h-p$ Versions. Part 3. The Adaptive $h-p$ Version, Numer. Math.,49, 577-612, 613-657, 659-683, 1986

[2] L. Demkowicz, A. Bajer and K. Banas, Geometrical Modeling Package, TICAM Report, University of Texas at Austin, 02-06, 1992

[3] C. J. Nedelec, "Mixed Finite Elements in R^3, Numer. Math., 35, 315-341, 1980

[4] C. J. Nedelec, A New Family of Mixed Finite Elements in R^3, Numer. Math, 50, 57-81, 1986

[5] L. Demkowicz, P. Monk, L. Vardapetyan and W. Rachowicz, De Rham Diagram for hp Finite Element Spaces, TICAM Report 99-06, 1999

[6] Ch. Schwab, p- and hp- Finite Element Methods, Oxford Science Publications

[7] W. Rachowicz and L. Demkowicz, An hp-Adaptive Finite Element Method for Electromagnetics, Int. J. Numer. Meth. Eng, 53, 147-180, 2002

[8] W. Rachowicz and L. Demkowicz, A Two-Dimensional hp-Adaptive Finite Element Package for Electromagnetics (2Dhp90_EM), Ticam Report , 16, 1998

[9] L. Demkowicz, 2D hp-Adaptive Finite Element Package(2Dhp90) Version 2.0, TICAM Report, University of Texas at Austin, 02-06, 2002

[10] L. Demkowicz, D. Pardo and W. Rachowicz, 3D hp-Adaptive Finite Element Package(2Dhp90), TICAM Report, University of Texas at Austin, 02-24, 2002

[11] D. Xue and L. Demkowicz, Geometrical Modeling Package Version 2.0, TICAM Report, University of Texas at Austin, 02-30, 2002

[12] Saikat Dey, Mark S. Shephard and E. Joseph Geometry Representation Issues Associated with p-Version Finite Element Computations, Rensselaer SCOREC report, 4, 1997

[13] Y. C. Chang and L. Demkowicz, Solution of Viscoelastic Scattering Problems in Linear Acoustics Using hp Boundary/Finite Element Method, International for Numerical Methods in Engineering, 44,12, 1885-1907, 1999

[14] A. Düster, High order finite elements for three-dimentional, thin-walled nonlinear continua, PhD dissertation, Shaker Verlag, 2002

[15] X. J. Luo, M. S. Shephard and J. F. Remacle, The Influence of Geometric Approximation on the Accuracy of High Order Methods, Rensselaer SCOREC report, 1, 2001

[16] X. J. Luo, M. S. Shephard and J. F. Remacle, p-Version Mesh Generation Issues, Rensselaer SCOREC report, 1, 2001

[17] Y. Zhang, C. Bajaj and B-S. Sohn, Adaptive and Quality 3D Meshing from Imaging Data, Proceedings of 8th ACM Symposium on Solid Modeling and Applications, June 16-20, 286-291, 2003

[18] Y. Zhang, C. Bajaj and B-S. Sohn, 3D Finite Element Meshing from Image Data, The special issure of Computational Methods in Applied Medhanics and Engineering on unstructral mesh generation, 2003

[19] L. Xue, L. Demkowicz and C. Bajaj, Reconstruction of G^1 surfaces with biquartic patches for *hp* FE simulations, 13th international meshing roundtable, 13, 323-332, 2004
[20] C. Bajaj and I. Lhm, Smooth Polyhedra using Implict Algebraic Splines, Computer Graphics, 79-88, July 1992
[21] L. Demkowicz, Projection-Based Interpolation, ICES reports, 3, 2004
[22] L. Demkowicz and A. Buffa, $H^1, H(curl)$ and $H(div)$-Conforming Projection-Based Interpolation in Three Dimensions. Quasi Optimal p-Interpolation Estimates, ICES Report, 24, 2004
[23] L. F. Demkowicz, A. Karafiat and J. T. Oden, On the Weak Form of Hypersingular Formulation for Scattering Problems in Linear Acoustics, TICOM Report, 1, 1991
[24] P. M. Morse and J. Feshbach, Methods of Theoretical Physicals, McGraw-Hill, 1, 1953

Department of Engineering Mechanics, University of Texas at Austin, TX, 78712
E-mail: `cynthia@ices.utexas.edu`
URL: `http://www.ices.utexas.edu/ cynthia`

Institute of Computational Engineering and Science, University of Texas at Austin, TX, 78712
E-mail: `leszek@ices.utexas.edu`
URL: `http://www.ices.utexas.edu/ leszek`